Spectroscopic Characterization of Active Mutants of Manganese Peroxidase: Mutations on the Proximal Side Affect Calcium Binding of the Distal Side†

Lucia Banci,‡ Ivano Bertini,*,‡ Cristina Capannoli,‡ Rebecca Del Conte,‡ and Ming Tien§

Department of Chemistry, Centro di Risononze Magnetiche, University of Florence, Florence, Italy, and Department of Biochemistry and Molecular Biology, The Pennsylvania State University, University Park, Pennsylvania 16802

Received October 27, 1998; Revised Manuscript Received May 10, 1999

ABSTRACT: The mutants at position 242 of manganese peroxidase (MnP), where the native Asp has been substituted with a Ser or a Glu, have been shown to be active, and are here characterized by electronic, EPR, and NMR spectroscopies. We have also mutated another residue on the proximal side, Phe 190 to Val and Leu, yielding active mutants. When studied by the above-mentioned spectroscopies, the mutants at both positions 242 and 190 exhibit three pH-dependent transitions. In contrast to the transitions observed at low and high pH, the spectroscopic studies reveal that the transition at intermediate pH has pK_a values up to 2 units lower for the mutants at D242E and -S and F190V than for the wild type. This process is due to the ionization of a group that affects the transition to the bis-histidine coordination at the iron. The observed changes in the pK_a values are related to the altered affinity of the calcium-binding site in the distal pocket. Other variations are observed in the other two pK_a values. Characterization of the cyanide derivatives indicates that the location and orientation of the distal and proximal His residues are essentially identical to that in the wild type. Our results indicate that mutations on the proximal side residues can affect changes in the distal side. In particular, deprotonation of a group, whose pK_a is influenced by the nature of the residues in the proximal side, produces a movement of helix B, which in turn induces the coordination of the distal His and the loss of the distal calcium ion.

Lignin (LiP)[1] and Mn peroxidases (MnP) are heme proteins produced by lignin-degrading fungi (*1*−*3*). They are structurally and mechanistically similar to plant and microbial peroxidases, such as horseradish peroxidase (HRP) and cytochrome *c* peroxidase (CcP). All of these enzymes utilize H_2O_2, also produced by ligninolytic fungi (*4*, *5*), to oxidize a variety of organic and inorganic substrates. Unique to these fungal peroxidases is their ability to oxidize substrates that other peroxidases cannot oxidize, due to their high reduction potential (*6*). MnPs, more prevalent in lignin-degrading fungi (*7*, *8*), are capable of directly oxidizing Mn^{2+} to Mn^{3+} (*9*). Mn^{3+} is a diffusible oxidant, thus being able to deliver the oxidizing potential of the heme active site to distant substrates such as lignin.

The structural aspects that confer upon these fungal peroxidases their potent reactivity, despite being homologous in structure to HRP and CcP, are not well understood. Past studies, both on synthetic heme models and on enzyme structure−function relationships, have focused on the coordination of the heme iron. Indeed, close examination of the structure of LiP, MnP, and CcP reveals that the hydrogen-bonding network of CcP differs from that of LiP and MnP (*10*−*13*). In CcP, the heme iron is coordinated to the proximal His which is hydrogen bonded to an Asp which in turn is hydrogen bonded to a Trp (*10*). Both LiP and MnP differ in that a Phe replaces the Trp, which is not capable of hydrogen bonding (*11*−*13*).

We have developed a heterologous expression system for MnP in *Escherichia coli* (*14*, *15*) which produces a non-glycosylated recombinant enzyme. We have used this system to mutate both the Asp242 and the Phe190 of MnP to obtain potentially all 19 mutations and screen for active mutants (see ref *51*). Two active mutants at residue Asp242, Asp242Glu and Asp242Ser, were obtained from the screen. With Phe190, three active mutants, Phe190Val, Phe190Leu, and Phe190Trp, were isolated. The Phe190Trp mutant is too unstable to permit reproducible spectroscopic characterization. The thoroughness of the selection process is based on a statistical argument using degenerate oligonucleotides. Thus, we cannot claim that the ones we isolated are the only active mutants. Indeed, Kishi et al. (*16*) isolated four active mutants at the Phe190 position.

In this paper, we describe the spectral characterization of the two Asp242 mutants and the two stable Phe190 mutants. Some properties of the Phe190Leu MnP mutant have already been reported (*16*). These studies are extended here, and from

† This research has been funded, in part, by Department of Energy Grant DE-FG02-87ER13690, "Foundations for controlling properties of haem proteins: structure/function relationships in archetypal systems and the development of an interdisciplinary methodology", ERB FMRX CT 98 0218, CNR-Progetto Finalizzato Biotecnologie 97.01027.49, and the Progetto Strategico "Tecnologie Chimiche Innovative" (95.04535.ST74).

* To whom correspondence should be addressed. Phone: +39.055.4209272. Fax: +39.055.4209271. E-mail: bertini@cerm.unifl.it.

‡ University of Florence.

§ The Pennsylvania State University.

[1] Abbreviations: LiP, lignin peroxidase; MnP, manganese peroxidase; CcP, cytochrome *c* peroxidase; HRP, horseradish peroxidase; MnPWT, fungal wild-type manganese peroxidase; rMnPWT, recombinant manganese peroxidase.

10.1021/bi9825697 CCC: $18.00
Published on Web 07/03/1999

these data, we infer aspects of the structural changes caused by these mutations.

EXPERIMENTAL PROCEDURES

Enzyme Production and Purification. The mutagenesis, expression, and purification of the recombinant proteins are as described by Whitwam et al. (*15*, *51*). The purified MnP had an R_z of ≥ 4.5. The enzyme concentration was determined using the extinction coefficient at 407 nm of 127 mM^{-1} cm^{-1} (*18*).

Electronic Spectroscopy. Electronic absorption spectra were obtained with a computer-interfaced Varian Cary 3 spectrophotometer. The pH titrations were performed in 50 mM phosphate or 25 mM MES buffer and by adjusting the pH with potassium hydroxide or hydrochloric or phosphoric acid. Where indicated, calcium ion was added as calcium chloride to a final concentration of 1.5 mM.

Electron Paramagnetic Resonance Spectroscopy. All EPR spectra were acquired using a Bruker model ER 200 spectrometer, operating at microwave frequency of 9.6 GHz, equipped with an Oxford cryostat. Enzyme samples were typically at a concentration of 1 mM in 50 mM potassium phosphate (pH 6.1). The cyanide adducts were obtained by adding a stoichiometric quantity of KCN.

Nuclear Magnetic Resonance. The effects of pH on the ^{1}H NMR spectra were determined with a Bruker MSL 200 spectrometer at 298 and 303 K. A super WEFT pulse sequence (*19*) was used with recycle delays of 100 and 350 ms. ^{1}H NMR spectra were also recorded with Bruker DRX 500 and AMX 600 spectrometers using a ^{1}H presaturation sequence and a recycling time of 350 ms at 298 K. The protein concentrations were 0.7−1.0 mM.

To enhance the detection of cross-peaks between signals with short T_1 values, NOESY spectra (*20*, *21*) were recorded at 500 MHz using a mixing time of 15 ms at 298 and 303 K. A total of 512 spectra were collected with 1K data points in the F_2 direction. The data were multiplied in both dimensions by a sine-squared bell window function with a phase shift of 45° and were zero-filled to obtain 1K × 1K real data points.

RESULTS

Spectroscopic Characterization. In MES buffer (pH 6.1), the electronic spectra of the rMnPWT and its mutants are indistinguishable from that of MnPWT (*22*). The spectra exhibit the Soret band at 407−408 nm and two charge-transfer bands (CT1 and CT2) at 502−504 and 636−637 nm, respectively. These spectra are typical of high-spin five-coordinate iron(III) heme systems. In contrast, the spectra of the mutants at the same pH of 6.1 except now in phosphate buffer reveal the appearance of a shoulder at 360 nm. Also apparent in some of the mutants are one or two absorptions, termed α and β, at 533−535 and 560−565 nm, respectively. These latter features indicate the presence of some low-spin iron(III) species (*23*). This behavior is not observed in rMnPWT or in MnPWT (*16*). The wavelengths of these transitions for the various enzyme preparations are listed in Table 1.

The ^{1}H NMR spectra of these mutant enzymes at pH 6.1 in MES buffer are shown as traces d and e of Figure 1. Also shown in Figure 1 is the spectrum of the rMnPWT (Figure 1a) which is identical to the spectrum of the MnPWT (*24*, *25*). All the spectra are similar and characteristic of a high-spin species exhibiting four downfield-shifted signals with intensity corresponding to three protons and shift values in the 80−60 ppm range. The signals of the four heme methyl groups can be assigned by comparison to our previous results with MnPWT (Table 2) (*24*, *25*). Specifically, the most downfield-shifted signal is likely to be due to 8-CH_3 and the following signal to 3-CH_3. Other single-proton intensity signals are detected which arise from protons of the heme substituents in the α position and to the βCH_2 protons of the proximal His. It is interesting to note that the average shift value of the four-methyl signals is slightly lower for the Asp242 mutants than for the rMnPWT enzyme. This may be the result of a different donor strength of the axial His. Boersma and Goff (*26*) have shown that the lower the imidazolate character, the higher the quantum mechanical mixing of the $S = {}^3/_2$ and ${}^5/_2$ states and the smaller the hyperfine shift.

Table 1: Electronic Transitions of MnP and Its Mutants[a]

enzyme	δ	Soret	CT2	β	α	CT1
MnPWT[b]		407	504			637
rMnPWT		407	504			637
MnPD242E	(360)	408	503	(535)	(560)	636
MnPD242S	(360)	408	502	(535)	(565)	636
MnPF190V	(360)	407	504	(533)		636
MnPF190L	(360)	407	504	(535)		637

[a] The values are in nanometers. The spectra were recorded in 25 mM MES buffer at pH 6.1. The further bands appearing in 50 mM potassium phosphate buffer at pH 6.1 are reported in parentheses. [b] Taken from ref *22*.

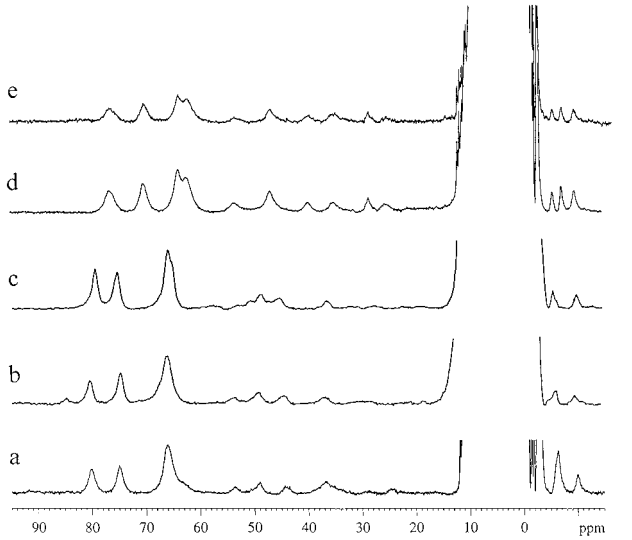

FIGURE 1: ^{1}H NMR spectrum at 600 MHz of rMnPWT (a), F190LMnP (b), F190VMnP (c), D242SMnP (d), and D242EMnP (e) in MES buffer at pH 6.1 and 298 K.

The EPR spectra of rMnPWT and the mutants were recorded at 4 K in MES buffer (pH 6.1). A representative spectrum of these enzymes, that of Asp242Ser, is shown in Figure 2a. The spectra of the various mutants and wild-type enzyme all exhibit a single high-spin axially symmetric species (*27*). All of the *g* values, as shown in Table 3, are very close. This suggests that the electronic structure of iron(III) in the mutants is similar to that of rMnPWT under the conditions used in the study.

Table 2: ^{1}H NMR Chemical Shift Values for Various MnPs in MES Buffer at pH 6.1 and 298 K

	MnPWT shift (ppm)[a]	rMnPWT shift (ppm)	MnPD242E shift (ppm)	MnPD242S shift (ppm)	MnPF190V shift (ppm)	MnPF190L shift (ppm)
8-CH_3	83.5	80.2	76.2	76.4	79.5	80.5
3-CH_3	77.5	75.0	70.0	70.1	75.7	74.9
5-CH_3	68.0	66.0	63.7 or 62.0	63.7 or 62.1	66.4 or 65.0	66.2
1-CH_3	68.0	66.0	63.7 or 62.0	63.7 or 62.1	66.4 or 65.0	66.2
7-H_α	61.0					59.1
7-$H_{\alpha'}$	51.0	49.0	46.8	46.6	48.9	49.2
2-H_α	37.5	37.0	35.1	35.1	37.1	37.2

[a] See ref *24*.

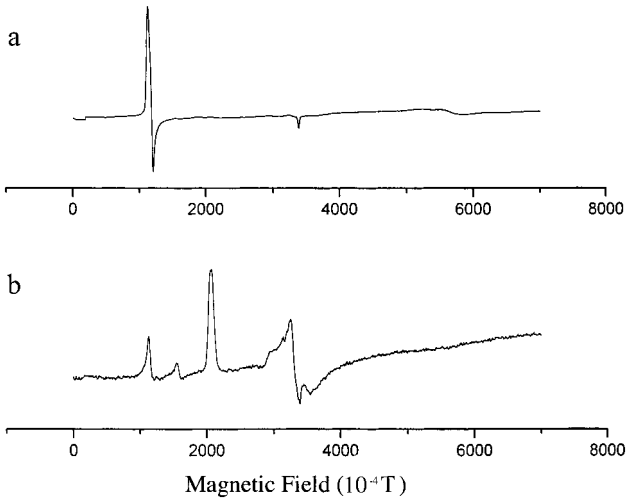

FIGURE 2: EPR spectra of D242SMnP (a) and D242SMnP-CN^- (b) recorded at 4 K in MES buffer at pH 6.1.

Table 3: *g* Values of EPR Spectra of rMnPWT and Some of Its Mutants and Their Cyanide Adducts, Recorded at 4 K in MES Buffer at pH 6.1

enzyme	*g* values
MnPWT	6.01, 1.99
rMnPWT	5.97, 2.00
MnPD242E	6.01, 2.00
MnPD242S	5.97, 2.00
MnPF190V	5.97, 2.00
MnPF190L	5.98, 1.99
MnPWT-CN^-	3.23, 2.21, 1.77
rMnPWT-CN^-	3.30, 2.06, −
MnPD242E-CN^-	3.10, 2.00, 1.21
MnPD242S-CN^-	3.27, 2.05, 1.22
MnPF190V-CN^-	3.21, 2.01, −
MnPF190L-CN^-	3.18, 2.07, −
alkaline form of MnPD242E	2.94, 2.30−5.96, 2.00

Effect of pH on the Spectral Properties. The pH dependence of the electronic spectra was studied in phosphate and MES buffers. Like those of native MnP (*16*), the electronic spectra of rMnPWT and its mutants are pH-dependent. Figure 3 shows the electronic spectrum of the Asp242Glu mutant, recorded at three different pH values. Increasing the pH above 6.1 in phosphate buffer caused a blue shift from 408 to 412 nm and a decrease in the intensity of the Soret transition. This was observed in all of the mutant enzymes. Furthermore, the shoulder at 360 nm and the α and β bands increase in intensity, and the latter two bands shift slightly in their absorption maximum to 530 and 565 nm, respectively. These electronic transitions (Figure 3b) are typical of a six-coordinate low-spin iron(III) species, characterized by bis-histidine coordination (*23*, *28*, *29*). Similar changes

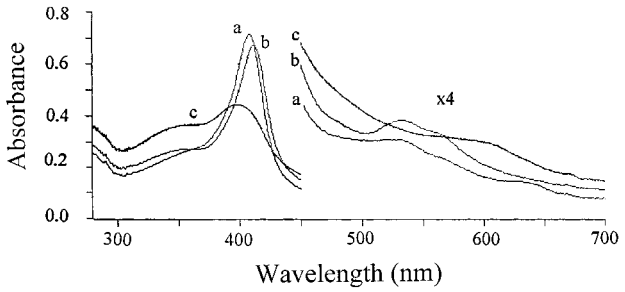

FIGURE 3: Electronic absorption spectra of the MnPD242E in 50 mM potassium phosphate buffer, recorded at pH 6.1 (a), 7.5 (b), and 10.2 (c).

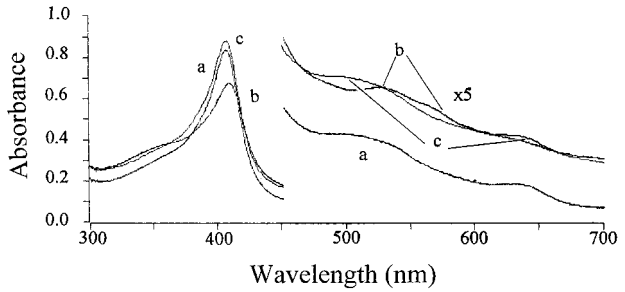

FIGURE 4: Electronic absorption spectra of the D242EMnP: (a) freshly purified, (b) after the sample has been taken to alkaline pH, and (c) like the conditions for spectrum b but after the addition of calcium. The protein is in 50 mM phosphate buffer at pH 6.1.

are also observed for MnPWT and rMnPWT. However, for the Asp242Ser, Asp242Glu, and Phe190Val mutants, the transition to this complex occurs at much lower pH values than in rMnPWT and Phe190Leu. Electronic spectra shown in Figure 3 (trace b), characteristic of a low-spin heme iron-(III) ion with bis-histidine coordination, have been previously observed for the MnP Asp47Ala mutant and for the thermally inactivated rMnPWT (*30*). Asp47 is a ligand for the distal calcium (*12*), and mutation at this site to an Ala results in the loss of this calcium. Thermal inactivation also results in the loss of this distal calcium (*30*).

Lowering the pH back to 6.1 after subjecting these mutants (F190V, D242S, and D242E) to alkaline pH did not result in recovery of the original spectrum (data not shown). The spectrum still maintained the features typical of the bis-histidine form, suggesting that the loss of calcium is not reversed under these conditions. However, the original spectrum can be recovered upon addition of calcium chloride (Figure 4) as previously shown by Sutherland et al. (*30*). Omission of calcium by adding sodium chloride did not cause the same transition. In contrast, MnPWT and MnPF190V exhibit fully reversible spectroscopic changes.

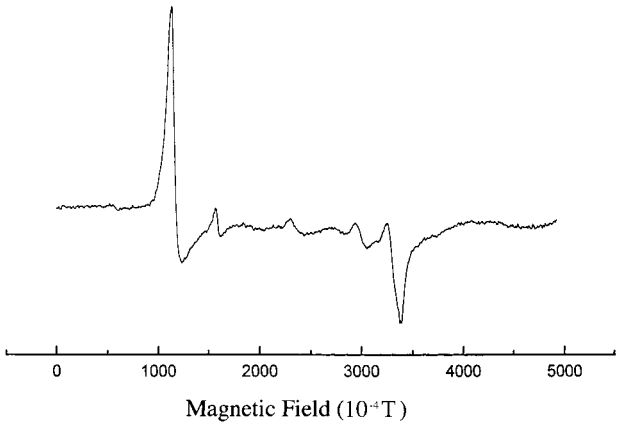

FIGURE 5: EPR spectra of the D242EMnP taken at alkaline pH (7.5) and back to pH 6.1 at 4 K in MES buffer.

The Asp242Ser mutant was further characterized by EPR spectroscopy at 4 K. The spectrum of this mutant, when taken at pH 7.5 and back to pH 6.1 but without addition of calcium chloride, exhibits the typical low-spin heme iron signals ($g = 2.94$ and 2.30, and the third g value was not detected due to its broad feature). The spectrum also shows the presence of trace amounts of high-spin iron(III) (at 5.96 and 2.00) (Figure 5 and Table 3) (*30*−*32*). The g values of the alkaline, low-spin form are similar to those reported for protein and synthetic bis-histidine heme complexes (*30*). The alkaline form has, with respect to the cyanide adducts, a smaller magnetic anisotropy which is consistent with the NMR spectra (see below).

Above pH 7 for the mutants and above pH 8.5 for the rMnPWT, in phosphate buffer, a blue shift and further reduction in Soret intensity are observed. The solution's color also changed from brown to green. The spectral changes observed between pH 7 and 10 are completely reversible; when the pH is lowered back to 7 from 10, the original spectrum is observed. The spectrum observed at this higher pH still reveals the presence of a low-spin six-coordinate iron(III).

Table 4: Apparent pK_a Values of Ionizations Affecting Electronic Spectra of Wild-Type and Mutant rMnP[a]

enzyme	pK_a1	pK_a2	pK_a3
rMnPWT	6.79 ± 0.08	8.53 ± 0.02	9.12 ± 0.22
MnPD242E	5.86 ± 0.10	6.46 ± 0.01	8.67 ± 0.05
	(6.32 ± 0.11)	(7.15 ± 0.02)	(8.85 ± 0.05)
MnPD242S	5.94 ± 0.03	6.46 ± 0.01	9.06 ± 0.05
	(5.85 ± 0.05)	(7.86 ± 0.02)	(9.05 ± 0.04)
MnPF190V	5.83 ± 0.02	6.19 ± 0.03	8.82 ± 0.08
	(5.90 ± 0.06)	(7.16 ± 0.04)	(8.65 ± 0.04)
MnPF190L	5.55 ± 0.10	8.35 ± 0.10	−
	(5.60 ± 0.08)	(−)	(9.50 ± 0.05)

[a] Spectra were recorded at 298 K in 50 mM phosphate buffer and in 25 mM MES buffer (values in parentheses).

The pH-dependent changes in the absorbance at 407 nm in phosphate buffer are shown in Figure 6. The calculated pK_a values, obtained from fitting the data to three single-proton processes, are listed in Table 4. The decrease in the Soret intensity at pH <6.1, observed for rMnPWT and Phe190Leu, has been previously reported (*16*) and is not fully understood. A decrease of approximately 2 pH units for the second transition (pK_a2), with respect to rMnPWT and Phe190Leu, is observed with the other mutants. An approximately 2 unit decrease in the pK_a2 values for the alkaline transition was also observed for CcP mutants of the same residue (i.e., the proximal Asp 235) (*23*, *28*).

In MES buffer, the Asp242Ser, Asp242Glu, and Phe190Val mutants still exhibit the pH-dependent spectral transition similar to that observed in phosphate buffer. However, the pK_a of the second transition was shifted to higher values (Figure 7). Again, the original species observed at pH 6.1 can be recovered from the alkaline form by lowering the pH (back to 6.1) and by adding calcium chloride. In contrast, the rMnPWT and the Phe190Leu mutant do not appear to lose their calcium ion either MES or phosphate buffer. Thus, it appears that the mutant enzymes are more stable in MES buffer and the loss of calcium ions occurs at higher pH values, if it occurs at all.

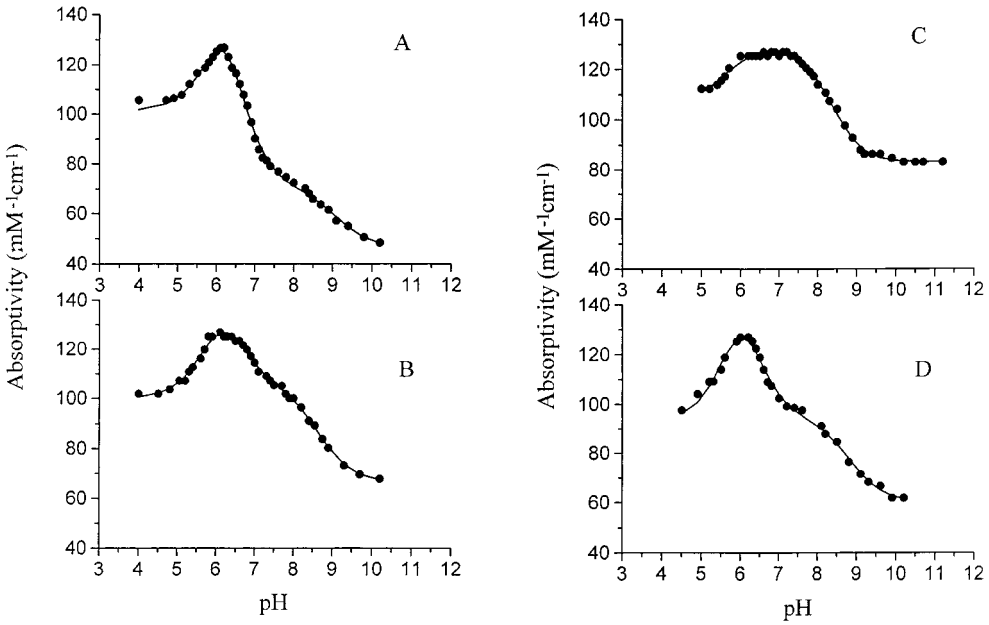

FIGURE 6: Dependence of the absorbance at 407 nm on pH in 50 mM phosphate buffer for D242SMnP (A), D242EMnP (B), F190LMnP (C), and F190VMnP (D). The solid lines represent the best fitting of the dependence.

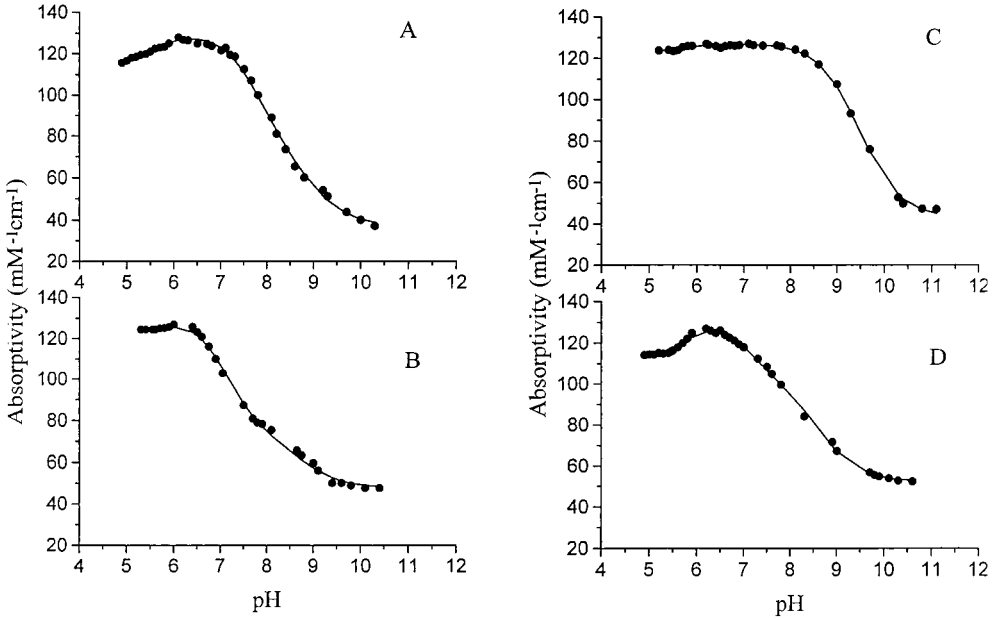

FIGURE 7: Dependence of the absorbance at 407 nm on pH in MES buffer for D242SMnP (A), D242EMnP (B), F190LMnP (C), and F190VMnP (D). The solid lines represent the best fitting of the dependence.

The instability of concentrated protein solutions in phosphate buffer at alkaline pH prevents NMR characterization. This again is most likely due to the loss of calcium (as calcium phosphate). In contrast, the samples were stable in MES buffer. By increasing the pH to 7.5, we detected very broad signals from the high-spin iron(III) species in the 80−60 ppm region of the ^{1}H NMR spectrum. When the pH is further increased, the signals of the high-spin form disappear, but no detectable resonances are observed for the low-spin iron(III) species. The ^{1}H NMR signals of the high-spin form reappeared by when the pH was lowered and calcium chloride was added. These results from the NMR studies, with regard to the effect of pH, are consistent with results obtained from electronic spectroscopy.

When the spectrum of the Asp242Glu mutant is recorded at pH 8.2 and at a lower temperature (289 K), the high-spin signals regain partial intensity. This is in contrast to the spectra recorded at 298 K which do not exhibit any high-spin signals. The other mutants have a similar temperature-dependent behavior. This behavior indicates that the pK_a for the bis-histidine transition is temperature-dependent, exhibiting a positive ΔH of ionization which is consistent with a decrease in pK_a as the temperature decreases. The disappearance of the NMR lines is unexpected for low-spin iron(III) systems, as they exhibit favorable electron relaxation, producing relatively small line broadening. However, previous studies have already shown that either a severe broadening or disappearance of the lines occurs for peroxidases when the bis-histidine coordination is formed (*28*, *33*). This signal disappearance could be due to conformational equilibrium on the time scale of 1000 s^{-1}, which is the range of the expected chemical shift separation between the two extreme forms. The concomitant loss of calcium could be the cause of protein flexibility in the distal side. Indeed, MD simulations (*34*) reveal that when the calcium ion is not added to the system during the simulations, the conformation of the distal His becomes quite unstable and experiences a large degree of flexibility.

The low-pH behavior of the NMR spectra is again consistent with the observation derived from electronic spectra that indicated no change in the spin state of the iron.

NMR and EPR Spectroscopy of the Cyanide Adducts. MnP, like other peroxidases, binds cyanide stoichiometrically (*25*) to produce a low-spin iron(III) form. Due to the faster electronic relaxation rates of the iron, which induce smaller signal line widths, the cyanide adduct is more suitable for NMR characterization than the high-spin form. Bound cyanide forms a hydrogen bond with the distal His that links it to the iron ion. This creates a network linking the proximal and distal sides. The ^{1}H NMR shift values of the cyanide adducts of rMnPWT and its mutants, as well as of LiP, are summarized in Table 5. The ^{1}H NMR spectrum of rMnPWT is indistinguishable from that of the native protein. The assignments shown in Table 5 have been either verified through two-dimensional NOESY experiments or assigned by analogy when the signal is identical to that of the wild-type protein. Analysis of these spectra reveals that (i) the orientation of the proximal His plane is the same among the mutants, (ii) the steric arrangement of the vinyl groups is the same, and (iii) the distal His has the same orientation as in MnPWT. The orientation of the imidazole plane of the proximal His determines the proton shifts of the groups attached to the heme moiety. Thus, the shifts of the 3-CH_3 and 8-CH_3 protons, which are the most shifted, are the most sensitive to minor structural changes. The change in the shift value of 3-CH_3 along the series of these MnP mutants is well below 10%. When the shift of 3-CH_3 increases, the shift of 8-CH_3 decreases as well (and that of Hϵ1 of the proximal His increases in absolute value). This is consistent with a rotation of a few degrees of the proximal His plane, from the N (pyrrole I)−N (pyrrole III) direction toward the meso−meso direction. Indeed, from spin density calculations, it has been found that a variation of 10% in the 8-CH_3 shifts [when the His plane is making an angle of ∼20° with the N (pyrrole I)−N (pyrrole III) direction] should correspond to a 5° rotation of the His plan toward the meso−meso direction (*35*).

Table 5: Chemical Shift Values for the Cyanide Adducts of rMnP and Fungal LiP[a]

	signal	MnPWT shift (ppm)[b]	rMnPWT shift (ppm)	MnPD242E shift (ppm)	MnPD242S shift (ppm)	MnPF190V shift (ppm)	MnPF190L shift (ppm)	LiP shift (ppm)[c]
2-H_α	J	8.6					8.5	8.4
2-$H_{\beta cis}$	X	−3.4	−3.2	−3.2		−3.3	−3.3	-3.5
2-$H_{\beta trans}$	Y	−3.2	−3.0	−3.0		−3.1	−3.1	-3.8
α-meso	α	−1.1		−1.0	−1.2	−0.7	−1.1	1.1
3-CH_3	A	30.7	30.8	28.4	28.7	30.2	30.6	30.1
4-H_α	E	12.7	13.1	12.9	12.9	13.1	12.9	13.8
4-$H_{\beta cis}$	W	−2.8	−2.8	−2.7	−2.7	−2.7	-2.8	-3.1
4-$H_{\beta trans}$	V	−1.8	−1.9	−1.9	−2.0	−2.0	-1.8	-1.8
7-H_α	D	12.5	12.8	12.9		12.6	12.6	11.6
7-$H_{\alpha'}$	I	8.0					8.3	10.1
8-CH_3	B	20.4	21.2 (21.5)	21.5	21.5	20.6	21.0	20.5
δ-meso	δ	7.0					6.8	7.4
NH_p p-His[d]	d	12.4	12.4	12.2	12.3	12.1	12.3	11.4
Hβ p-His	C	19.5	19.3			19.5	19.3	17.0
Hβ′ p-His	F	16.9	16.9	16.8	17.0	16.1	16.8	16.5
Hδ1 p-His	f	15.1	15.0	15.7	16.0	14.6	14.9	14.0
Hε1 p-His	Z	−11.8	−11.0	−14.9	−15.0	-13.3	-12.1	-8.4
Hδ2 p-His	H′	20.3	21.2 (21.0)	21.4	22.7	20.4	20.7	13.3
Hε1 d-His								13.4
Hε2 d-His	a	34.2	33.7	34.1	34.1	33.6	33.8	35.2
Hδ1 d-His		17.0	17.2	17.1	17.1	17.0	16.8	17.0

[a] Spectra were obtained in 50 mM phosphate buffer at pH 6.1 and 298 K. [b] See refs *24* and *25*. [c] See refs *49* and *50*. [d] p-His and d-His are proximal His and distal His, respectively.

The pattern of the shifts for Hα, Hβ_{trans}, and Hβ_{cis} of the vinyl group indicates that the conformation observed in the X-ray structure of MnPWT is maintained. The shifts of the distal His essentially arise from pseudocontact shifts (*36*), which are determined by the coordinates of the resonating nuclei within the molecular axes (determined by the magnetic susceptibility tensor principal directions). Therefore, the shifts of the protons of the distal His confirm the similarity in the structure of the mutants.

The EPR spectra of the cyanide adducts exhibit signals characteristic of low-spin iron(III) species (*30*). The *g* values are listed in Table 3. The spectra also show traces of high-spin iron(III) species. There is also a small signal at $g \approx 4.3$ which is commonly observed in many low-spin iron adducts. This signal has been identified to arise from traces of contaminating non-heme rhombic iron (*32*) (Figure 2b). For some of the adducts, the high magnetic field feature is not observed, due to its large line width. As the protein is very sensitive to the freezing process at 4 K, the observed *g* values can be considered unchanged and within the experimental error.

Cyanide Binding to MnP Mutants. The collective results suggest that mutations in the proximal side of the protein affect the properties of the distal side. The mutations apparently perturb calcium binding on the distal side in a pH-dependent manner. This, in turn, causes the distal His to be more readily available for coordination to the iron. This was further substantiated by equilibrium studies of cyanide binding. The affinity constant *K* for cyanide binding was determined at pH 4.4, 6.0, and 8.0 for both the rMnPWT and the Phe190Val mutant through spectroscopic titration with increasing amounts of cyanide. In agreement with previous results (*37*), the affinity constant for cyanide binding to rMnPWT did not change with pH, having a value of approximately 5×10^4 M^{-1}. For the Phe190Val mutant, a relatively small and insignificant decrease in affinity is observed by increasing the pH. However, as shown in Figure 8, a significant change in the amplitude of the absorbance change is observed in the Soret band. The amplitude is much smaller for the mutant enzyme at pH 8 than at pH 6 when compared to that of the wild-type protein. This behavior is consistent with cyanide binding only to the five-coordinate species but not to the bis-histidine complex.

To further verify this hypothesis, we studied the cyanide binding at pH 8 via NMR spectroscopy. The results indicate that at pH 8, a maximum of about 20% of the protein binds cyanide. This is most likely due to the strong bond between the iron and the distal His in the bis-histidine complex. Addition of cyanide does not displace the distal His, and therefore, the cyanide complex is not formed.

DISCUSSION

A variety of studies have shown that the heme environment of MnP is similar to that of other fungal and plant peroxidases. In addition to the proximal His173 and Asp242, there are two Phe residues near the active site (Phe190 and Phe45). The proximal Asp (Asp242), which is a conserved in all the peroxidases that have been sequenced, has been proposed to impart histidinate character to the proximal histidine by hydrogen bonding (*38*). This, in turn, is proposed to stabilize the higher oxidation states of the iron. These properties facilitate the formation and stabilization of compound I, in contrast to what is observed with myoglobin where the lower oxidation state, ferrous ion, is stabilized. More variability is observed with the proximal Phe residue. It is conserved in LiP, HRP (*11*−*13*), and peanut peroxidases (*39*) but not found in CcP (*40*) and ascorbate peroxidases (*41*), where a Trp is located at this position. In *Coprinus* peroxidase, the Phe is replaced by a Leu (*42*).

To study the role of Asp242 and Phe190 in MnP, we have characterized active mutants obtained from random mutagenesis and screening. The active mutant enzymes were due to relatively conservative mutations. For Asp242, we obtained mutations with Glu and Ser, both of which are capable of hydrogen bonding with the axial histidine. For

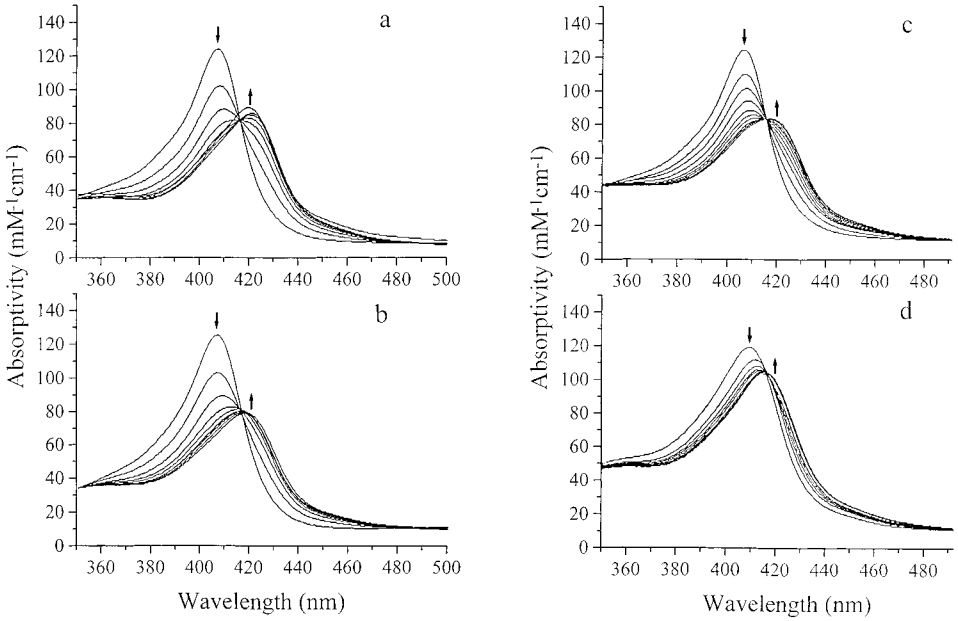

FIGURE 8: Electronic spectra, in 200 mM MES buffer, of cyanide titration of rMnPWT (a) and F190VMnP (b) at pH 6.0 and of rMnPWT (c) and F190VMnP (d) at pH 8.0. The arrows show direction of spectral change upon successive addition of potassium cyanide.

Phe190, we obtained mutations with Leu and Val (the Trp mutant was too unstable for characterization here); both are hydrophobic residues that presumably do not alter the stereochemistry of the surrounding of the iron. Indeed, the ^{1}H NMR data of the cyanide derivatives definitely demonstrate that the orientation of the histidine planes with respect to the heme moiety is maintained.

Electronic spectra and NMR spectra of heme proteins are indicators of the spin state of the heme iron(III). Coordination by strong-field ligands, such as cyanide or histidine, generates low-spin derivatives, whereas an empty coordination site or coordination of weak-field ligands, such as water, yields high-spin species. In the electronic spectra, iron heme proteins typically exhibit four bands in the visible region. Two bands, α and β, appear near 560 and 540 nm, respectively, and two ligand-to-metal charge-transfer (CT2 and CT1) bands occur near 500 and 630 nm, respectively (*43*). High-spin derivatives exhibit absorption maxima at the CT bands, whereas low-spin derivatives exhibit absorption maxima at α and β bands (*23*). At pH 6.1, the electronic spectra of the wild-type and mutant MnP indicate that the heme iron is predominantly in the five-coordinate high-spin state (*25*). In phosphate buffer at pH 6.1, a small fraction is in the six-coordinate low-spin state. The amount of the six-coordinate low-spin species is estimated to be $<10\%$. The EPR results, at liquid helium temperature, are consistent with this hypothesis. In fact, the spectra exhibit a single high-spin axially symmetric species, typical of high-spin MnP (*30*−*32*) (Table 3).

With increases in pH, all the MnP mutants and the wild type are converted to the six-coordinate low-spin species. The EPR spectra and the absorption spectra of these low-spin species are identical to those observed after the so-called "alkaline transition" in peroxidases. Such transition produces in all peroxidases with the exception of HRP, a bis-histidine coordination at the iron ion (*16*, *44*). The spectra are also identical to those of thermally inactivated MnP and of the Asp47Ala mutant of MnP, previously reported by Sutherland et al. (*30*). This mutation alters the distal calcium-binding site, resulting in the loss of calcium. Collectively, these data (in particular the data showing the decrease in the pK_a for the alkaline transition) suggest that the mutations at position 190 and particularly at position 242 influence the coordination of the heme iron, favoring the formation of the bis-histidine complex. The bis-histidine complex is apparently formed from the movement of the distal histidine toward the heme iron such that it, along with the proximal histidine (His46 and His173, respectively), forms a complexe with the iron. Our results indicate that the deprotonation of a group in the distal pocket can induce a movement in helix B, which contains His46 (*12*) such that it can now assume the correct position for coordination to the iron. This movement of helix B produces also a displacement of Asp47, which is adjacent to the distal histidine and is one of the calcium ligands. Movement of this residue could result in drastically reduced affinity for calcium ions.

In this study, we have shown that mutations in the proximal site can affect structural properties and pK_a values in the distal site. Proximal site mutations caused a decrease in the pK_a of an ionization responsible for the alkaline transition by 2 pH units (with the exception of Leu190). Our results do not allow us to determine how this change is propagated. However, the crystal structure reveals a chain of ordered, conserved water molecules and H-bonds connecting the proximal site with the distal sites of peroxidases (*11*, *34*). This chain of water molecules may be responsible for the transfer of structural and acid−base changes from the proximal to the distal site.

During our spectroscopic studies, we detected another pK_a at higher pH values. A similar pK_a has been observed in several other peroxidases as well as in their mutants, but has always been attributed to protein denaturation (*16*, *23*, *28*). The reversibility of the pH-dependent changes indicates an equilibrium between two species. The spectrum of these mutants at pH above 9 is very similar to that observed for thermally inactivated LiP. This observation has led to the

proposal that partial protein unfolding occurs, thus resulting in an increased degree of exposure of the heme to the solvent. The spectroscopic changes at this higher pH may reflect the coordination of an OH^- group. This is also consistent with the blue shift of the Soret band and an increase in the intensity of the α and β bands.

The electronic and ^{1}H NMR spectra indicate that the equilibrium occurring at low pH is between two high-spin species. A similar acidic pK_a has been observed in CcP and has been proposed to be caused by deprotonation of either a propionate group or the distal histidine despite the presence of other candidate acidic groups in the heme cavity (*45*, *46*). The MnP mutants studied here cannot be characterized at low pH as they are quite unstable and precipitate. The tendency to precipitate is only observed for the recombinant proteins as they approach their isoelectric point [for MnPWT, pI = 4.5 (*47*)]. Thus glycosylation may play a role in minimizing protein−protein interactions which result in precipitation.

Finally, a distinguishing feature of these mutants is that at high pH, conditions that favor formation of the bis-histidine complex, no hyperfine-shifted signal is observed. In contrast, for CcP (*28*, *45*) hyperfine-shifted signals have been observed with shift values typical for a low-spin iron(III). However, these signals are relatively broad compared to what is typically observed for other low-spin systems. In particular, the hyperfine-shifted signals of systems containing bis-histidine coordinated iron(III), such as cytochrome b_5, are quite sharp (*48*). This could be due to line broadening as a result of local mobility. The mobility detected through broadening of the NMR lines is faster than 1000 s^{-1}, which corresponds to the frequency separation between different possible conformations. The axial cyanide group stabilizes the proximal His−Fe−CN−distal His moiety and stabilizes a single conformation. As a result, the ^{1}H NMR spectra are well-resolved and informative. Comparison of these data with those from other peroxidases suggests that similar environments surrounding the heme iron are needed for the function of peroxidases since the shift pattern of all the cyanide derivatives of peroxidases and their active mutants exhibits very similar NMR shift patterns. The latter have been found to be sensitive to the orientation of the proximal His plane with respect to the heme moiety, thus indicating a very similar iron ligand orientation.

REFERENCES

1. Tien, M., and Kirk, T. K. (1983) *Science 221*, 661−663.
2. Glenn, J. K., Morgan, M. A., Mayfield, M. B., Kuwahara, M., and Gold, M. H. (1983) *Biochem. Biophys. Res. Commun. 114*, 1077−1083.
3. Paszczynski, A., Huynh, V.-B., and Crawford, R. (1985) *FEMS Microbiol. Lett. 29*, 37−41.
4. Faison, B. D., and Kirk, T. K. (1983) *Appl. Environ. Microbiol. 46*, 1140−1145.
5. Forney, L. J., Reddy, C. A., Tien, M., and Aust, S. D. (1982) *J. Biol. Chem. 257*, 11455−11462.
6. Kersten, P. J., Kalyanaraman, B., Hammel, K. E., Reinhammar, B., and Kirk, T. K. (1990) *Biochem. J. 268*, 475−480.
7. Kirk, T. K., and Farrell, R. L. (1987) *Annu. Rev. Microbiol. 41*, 465−505.
8. Orth, A. B., Royse, D. J., and Tien, M. (1993) *Appl. Environ. Microbiol. 59*, 4017−4023.
9. Glenn, J. K., Akileswaran, L., and Gold, M. H. (1986) *Arch. Biochem. Biophys. 251*, 688−696.
10. Poulos, T. L., and Kraut, J. (1980) *J. Biol. Chem. 255*, 8199−8205.
11. Poulos, T. L., Edwards, S. L., Wariishi, H., and Gold, M. H. (1993) *J. Biol. Chem. 268*, 4429−4440.
12. Sundaramoorthy, M., Kishi, K., Gold, M. H., and Poulos, T. L. (1994) *J. Biol. Chem. 269*, 32759−32767.
13. Piontek, K., Glumoff, T., and Winterhalter, K. (1993) *FEBS Lett. 315*, 119−124.
14. Pease, E. A., Aust, S. D., and Tien, M. (1991) *Biochem. Biophys. Res. Commun. 179*, 897−903.
15. Whitwam, R., and Tien, M. (1996) *Arch. Biochem. Biophys. 333*, 439−446.
16. Kishi, K., Hildebrand, D. P., Kusters-van Someren, M., Gettemy, J., Mauk, A. G., and Gold, M. H. (1997) *Biochemistry 36*, 4268−4277.
17. Banci, L., Rosato, A., and Turano, P. (1996) *JBIC, J. Biol. Inorg. Chem. 1*, 364−367.
18. Millis, C. D., Cai, D., Stankovich, M. T., and Tien, M. (1989) *Biochemistry 28*, 8484−8489.
19. Inubushi, T., and Becker, E. D. (1983) *J. Magn. Reson. 51*, 128−133.
20. Macura, S., Wuthrich, K., and Ernst, R. R. (1982) *J. Magn. Reson. 47*, 351−357.
21. Marion, D., and Wuthrich, K. (1983) *Biochem. Biophys. Res. Commun. 113*, 967−974.
22. Glenn, J. K., and Gold, M. H. (1985) *Arch. Biochem. Biophys. 242*, 329−341.
23. Vitello, L. B., Erman, J. E., Miller, M. A., Mauro, J. M., and Kraut, J. (1992) *Biochemistry 31*, 11524−11535.
24. Banci, L., Bertini, I., Pease, E. A., Tien, M., and Turano, P. (1992) *Biochemistry 31*, 10009−10017.
25. Banci, L., Bertini, I., Bini, T., Tien, M., and Turano, P. (1993) *Biochemistry 32*, 5825−5831.
26. Boersma, A. D., and Goff, H. M. (1982) *Inorg. Chem. 21*, 581−586.
27. Mino, Y., Wariishi, H., Blackburn, N. J., Loehr, T. M., and Gold, M. H. (1988) *J. Biol. Chem. 263*, 7029−7036.
28. Ferrer, J. C., Turano, P., Banci, L., Bertini, I., Morris, I. K., Smith, K. M., Smith, M., and Mauk, A. G. (1994) *Biochemistry 33*, 7819−7829.
29. Goodin, D. B., and McRee, D. E. (1993) *Biochemistry 32*, 3313−3324.
30. Sutherland, G. R. J., Zapanta, L. S., Tien, M., and Aust, S. D. (1997) *Biochemistry 36*, 3654−3662.
31. Wittenberg, B. A., Kampa, L., Wittenberg, J. B., Blumberg, W. E., and Peisach, J. (1968) *J. Biol. Chem. 243*, 1863−1870.
32. Blumberg, W. E., Peisach, J., Wittenberg, B. A., and Wittenberg, J. B. (1968) *J. Biol. Chem. 243*, 1854−1862.
33. Turano, P., Ferrer, J. C., Cheesman, M. R., Thomson, A. J., Banci, L., Bertini, I., and Mauk, A. G. (1995) *Biochemistry 34*, 13895−13905.
34. Banci, L., Carloni, O., Diaz, A., and Gori Savellini, G. (1996) *JBIC, J. Biol. Inorg. Chem. 1*, 264−272.
35. Shokhirev, N. V., and Walker, F. A. (1995) *J. Phys. Chem. 99*, 17795−17804.
36. Banci, L., Bertini, I., Pierattelli, R., Tien, M., and Vila, A. J. (1995) *J. Am. Chem. Soc. 117*, 8659−8667.
37. Cai, D. Y., and Tien, M. (1991) *J. Biol. Chem. 266*, 14464−14469.
38. Quinn, R., Mercer-Smith, J., Burstyn, J., and Valentine, J. S. (1984) *J. Am. Chem. Soc. 106*, 4136−4144.
39. Schuller, D. J., Ban, N., Huystee, R. B., McPherson, A., and Poulos, T. L. (1996) *Structure 4*, 311−321.
40. Finzel, B. C., Poulos, T. L., and Kraut, J. (1984) *J. Biol. Chem. 259*, 13027−13036.
41. Patterson, W. R., and Poulos, T. L. (1995) *Biochemistry 34*, 4331−4341.

42. Petersen, J. F., Tams, J. W., Vind, J., Svensson, A., Dalboge, H., Welinder, K. G., and Larsen, S. (1993) *J. Mol. Biol. 232*, 989−991.
43. Palmer, G. (1985) *Biochem. Soc. Trans. 13*, 548−560.
44. Smulevich, G., Miller, M. A., Kraut, J., and Spiro, T. G. (1991) *Biochemistry 30*, 9546−9558.
45. Bujons, J., Dikiy, A., Ferrer, J. C., Banci, L., and Mauk, A. G. (1997) *Eur. J. Biochem. 243*, 72−84.
46. Satterlee, J. D., and Erman, J. E. (1980) *Arch. Biochem. Biophys. 202*, 608−616.
47. Farrell, R. L., Murtagh, K. E., Tien, M., Mozuch, M. D., and Kirk, T. K. (1989) *Enzyme Microb. Technol. 11*, 322−328.
48. Banci, L., Bertini, I., Bruschi, M., Sompornpisut, P., and Turano, P. (1996) *Proc. Natl. Acad. Sci. U.S.A. 93*, 14396−14400.
49. Banci, L., Bertini, I., Turano, P., Tien, M., and Kirk, T. K. (1991) *Proc. Natl. Acad. Sci. U.S.A. 88*, 6956−6960.
50. de Ropp, J. S., La Mar, G. N., Wariishi, H., and Gold, M. H. (1991) *J. Biol. Chem. 266*, 15001−15008.
51. Whitwam, R. E., Koduri, R. S., Natan, M., and Tien, M. (1999) *Biochemistry 38*, 9608−9616.

BI9825697